HAC REF G4300

(2)

DTIC FILE COPY

AD-A198 481

AFOSR-TR- 88-0833

IONIZATION RATES RELEVANT TO LASER COOLING OF HYDROGEN

R. Steven Turley

Hughes Research Laboratories
3011 Malibu Canyon Road
Malibu, California 90265

June 1988

F49620-87-C-0083
Final Report
August 1, 1987 through January 31, 1988

UNITED STATES AIR FORCE, AFSC
AIR FORCE OFFICE OF SCIENTIFIC RESEARCH
Building 410
Bolling Air Force Base
Washington, D.C. 20332-6448

88 8

UNCLASSIFIED
SECURITY CLASSIFICATION OF THIS PAGE

REPORT DOCUMENTATION PAGE

Form Approved OMB No. 0704-0188

1a. REPORT SECURITY CLASSIFICATION: Unclassified	1b. RESTRICTIVE MARKINGS
2a. SECURITY CLASSIFICATION AUTHORITY	3. DISTRIBUTION/AVAILABILITY OF REPORT: Approved for public release, distribution unlimited
2b. DECLASSIFICATION/DOWNGRADING SCHEDULE	
4. PERFORMING ORGANIZATION REPORT NUMBER(S)	5. MONITORING ORGANIZATION REPORT NUMBER(S): AFOSR-TR- 88-0833
6a. NAME OF PERFORMING ORGANIZATION: Hughes Research Laboratories; 6b. OFFICE SYMBOL (If applicable): HRL	7a. NAME OF MONITORING ORGANIZATION: AFOSR/NP
6c. ADDRESS (City, State, and ZIP Code): 3011 Malibu Canyon Road, Malibu, CA 90265	7b. ADDRESS (City, State, and ZIP Code): Bolling Air Force Base, D.C. 20332-6448 (B1C141C)
8a. NAME OF FUNDING/SPONSORING ORGANIZATION: AFOSR; 8b. OFFICE SYMBOL (If applicable): NP	9. PROCUREMENT INSTRUMENT IDENTIFICATION NUMBER: F49620-87-C-0083
8c. ADDRESS (City, State, and ZIP Code): Bolling Air Force Base, D.C. 20332-6448 (B1C141C)	10. SOURCE OF FUNDING NUMBERS: PROGRAM ELEMENT NO. 61102F; PROJECT NO 2301; TASK NO A7; WORK UNIT ACCESSION NO

11. TITLE (Include Security Classification)
Ionization Rates Relevant to Laser Cooling of Hydrogen (U)

12. PERSONAL AUTHOR(S)
R. Steven Turley

13a. TYPE OF REPORT	13b. TIME COVERED	14. DATE OF REPORT (Year, Month, Day)	15. PAGE COUNT
Final	FROM 87/8/1 TO 88/1/31	1988 June	52

16. SUPPLEMENTARY NOTATION

17. COSATI CODES			18. SUBJECT TERMS (Continue on reverse if necessary and identify by block number)
FIELD	GROUP	SUB-GROUP	laser cooling, VUV Production, Neutral Particle Beams, Lyman-Alpha

19. ABSTRACT (Continue on reverse if necessary and identify by block number)

We have produced a VUV source suitable for atomic hydrogen cooling. The source is coherent, high intensity, narrowband, and broadly tunable around Lyman-α (1216 Å). We report the results of studying, characterizing, and optimizing this source for conditions important to laser cooling.

20. DISTRIBUTION/AVAILABILITY OF ABSTRACT: ☒ UNCLASSIFIED/UNLIMITED ☒ SAME AS RPT ☐ DTIC USERS	21. ABSTRACT SECURITY CLASSIFICATION: Unclassified
22a. NAME OF RESPONSIBLE INDIVIDUAL: Lt Col Bruce L. Smith	22b. TELEPHONE (Include Area Code): 202-767-4908; 22c. OFFICE SYMBOL: NP

DD Form 1473, JUN 86 — Previous editions are obsolete. — SECURITY CLASSIFICATION OF THIS PAGE: UNCLASSIFIED

TABLE OF CONTENTS

LIST OF ILLUSTRATIONS

LIST OF ILLUSTRATIONS (Continued)

SECTION 1

INTRODUCTION

Laser cooling of atomic hydrogen has practical importance in a wide variety of applications ranging from relativistic neutral particle beam weapons to atomic clocks and exotic fuels. A laser beam suitable for atomic hydrogen cooling needs to be high intensity, narrowband, coherent, and broadly tunable in the region around Lyman-α (1216 Å). We have produced a source meeting these criteria here at Hughes Research Laboratories (HRL). In the work funded by this contract, we studied, characterized, and optimized this source for conditions important to laser cooling.

In this introductory section, we will discuss the physics and potential practical applications of laser cooling and tunable VUV sources. These will be followed by an introduction to the specific results obtained during the six months of this contract.

1.1 REVIEW OF THE PHYSICS OF ATOMIC-BEAM/LASER INTERACTIONS

When an atom interacts with an external electromagnetic field, the center of mass motion of the atom is modified by the recoil of the atom when absorbing or emitting photons. Under appropriate conditions, the collective atomic recoil serves to reduce the momentum spread of an atomic sample (laser cooling).

In this subsection, we will review some physics necessary for understanding the most prominent features of this effect. In addition, we will present several techniques that could be used to cool an atomic sample.

The Hamiltonian for the interaction of an atom with a laser field can be written in the form,

$$H = H_O + H_I + H_F + H_{CM} \quad , \qquad (1)$$

where H_0 is the Hamiltonian for the internal atomic degrees of freedom. For the purposes of the following discussion, we will assume that the eigenstates of H_0 consist of two levels, a ground state $|a\rangle$, and an excited state $|b\rangle$ (see Figure 1). H_I represents the coupling between the electromagnetic fields and the atom. In the cases we will consider here, the dominant contribution to H_I is given by $H_I = -\vec{\mu}\cdot\vec{\mathcal{E}}$, where $\vec{\mu}$ is the atomic dipole moment and $\vec{\mathcal{E}}$ is the electric field. H_F is the free-field Hamiltonian for the electromagnetic field. H_{CM} represents the center of mass motion of the atom, where $H_{CM}=p^2/2m$.

In the low intensity limit, the eigenstates of the atomic and electromagnetic fields are decoupled, and the atomic eigenstates are independent of the intensity of the electromagnetic field. In the high intensity limit, the electromagnetic field serves to mix the unperturbed atomic eigenstates. This mixing can be most easily handled by replacing the "pure" atomic states with "dressed states" (eigenstates of the atom plus laser field system), which will be denoted as $|+,n\rangle$ or $|-,n\rangle$, where n is the photon number of the state.

The dressed states occur in doublets, each state consisting of a mixture of the two states $|a,n+1\rangle$ and $|b,n\rangle$. Let δ be the detuning--the difference between the laser frequency ω_L and the transition energy E_b-E_a. We will denote the Rabi flopping frequency as ω_R, where

$$\omega_R = \vec{\mu}\cdot\vec{\mathcal{E}}/ \qquad . \qquad (2)$$

The quantity $\vec{\mu}$ is the dipole interaction matrix element $e\langle b|\vec{r}|a\rangle$ and $\vec{\mathcal{E}}$ is the electric field vector. If the phase of the dipole interaction matrix element is chosen to be real, the mixing of

Figure 1. Two-level atom eigenstates and energy levels.

the two states is described by the intensity dependent expressions[1]

$$\begin{aligned} |+,n\rangle &= \cos(\theta)|a,n+1\rangle + \sin(\theta)|b,n\rangle \\ |-,n\rangle &= -\sin(\theta)|a,n+1\rangle + \cos(\theta)|b,n\rangle, \end{aligned} \tag{3}$$

where the mixing angle θ is defined by $\tan(\theta) = (\Omega-\delta)/\omega_R$ and Ω is defined to be $(\delta^2+\omega_R^2)^{1/2}$ The energies of the two eigenstates are

$$\begin{aligned} \frac{E^+}{h} &= (n+1)\omega_L - \frac{\delta}{2} + \frac{\Omega}{2} \\ \frac{E^-}{h} &= (n+1)\omega_L - \frac{\delta}{2} - \frac{\Omega}{2} \end{aligned} \tag{4}$$

1.1.1 Cooling Schemes

A number of schemes for cooling a gas take advantage of the exchange of momenta between photons and the constituent atoms of the gas. These schemes can be classified into the four general areas of collisional, spontaneous, stimulated, and π-pulse cooling. Realizations of each of these schemes will be discussed below.

1.1.1.1 Collisional Cooling. Figure 2 is an example of a collisional cooling scheme. A laser is tuned to the red side of an atomic resonance, exciting the atom from $|a\rangle$ to $|b\rangle$. The atom spontaneously decays from $|b\rangle$ to $|a\rangle$, losing an energy E_b-E_a, slightly more than the energy of the exciting laser. The difference in energy between the incident and radiated photons is provided by energy picked up during a collision with another atom. Thus, the total kinetic energy of the gas is decreased. Energy is lost in collisions with other atoms in the gas. This technique is the least efficient of the laser cooling prospects we will discuss. The change of atomic momentum per absorbed photon is typically a small fraction of the photon momentum.

16928-

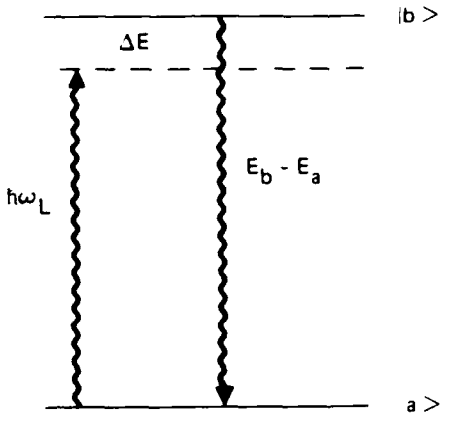

Figure 2. Collisional cooling scheme. The atom absorbs energy $\hbar\omega_L$ and emits energy E_b-E_a. The energy difference ΔE is carried away by a collision process.

1.1.1.2 Spontaneous Cooling. A much more efficient technique for cooling atoms is what we call spontaneous cooling. A group at the National Bureau of Standards was able to use this technique to cool a thermal beam of sodium atoms down to a temperature of 100 mK.[2] Figure 3 is an illustration of the technique we originally envisioned for transverse cooling of a relativistic atomic beam by spontaneous cooling. In this technique, two laser beams are incident on either side of the atomic beam to be cooled. The laser frequency ν is Doppler shifted to a new frequency ν' in the rest frame of the atom. If β is the speed of the atom in units of the speed of light, and $\gamma=(1-\beta^2)^{1/2}$, the frequency ν' is given by

$$\nu' = \gamma\nu[1-\beta\cos(\theta)] \quad . \tag{5}$$

As indicated in Figure 3, θ is the angle between the laser beam and the atomic velocity vector. In the nonrelativistic limit of velocities much slower than the speed of light, this expression reduces to

$$\nu - \nu' = \vec{k}\cdot\vec{v}/2\pi \quad , \tag{6}$$

where $\vec{k}$ is the wave vector of the laser beam.

Spontaneous cooling techniques take advantage of the inhomogeneous Doppler shift to cool the atoms in the beam. For simplicity, imagine a beam in which all of the atoms have a uniform speed, but slightly different trajectories. The $\cos(\theta)$ term of Eq. (5) will cause the resonant frequency of each atom to have an angle-dependent frequency shift. Thus the laser will only be resonant with atoms within a narrow angular range. These atoms will pick up one unit of photon momentum, $\hbar k$, as they absorb a photon from the laser beam. An equal amount of momentum

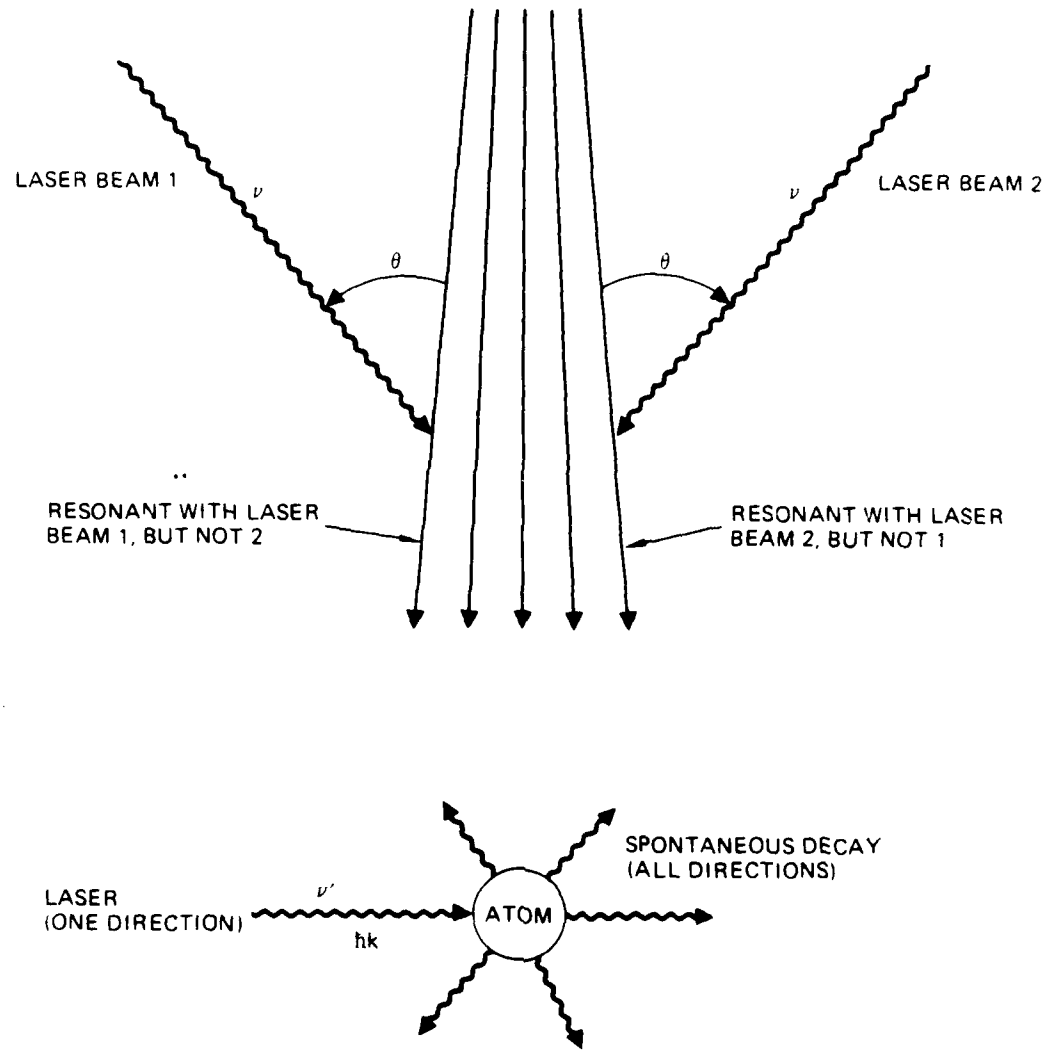

Figure 3. Spontaneous cooling scheme. Atoms moving toward laser beam 1 are resonant with it, but nonresonant with laser beam 2. They are "pushed" away from laser 1 by the recoil of the absorbed photon from laser 1. Since the atom scatters the absorbed photon into 4π, the net effect of the fluorescence is 0. Atoms moving toward laser beam 2 are likewise moved toward a central trajectory.

is lost when the photon is reradiated as the atom relaxes to the ground state. However, the photons absorbed from the laser are all in the same direction and their effect is cumulative. The photons radiated by the excited atoms are radiated into a 4π solid angle. The cumulative recoil from the radiated photons averages out to zero.

In Figure 3, atoms moving away from the central trajectories of the atomic beam will be "pushed" away from the laser beams they are moving toward. Atoms moving on the central trajectory or away from a particular cooling laser beam will be nonresonant with the laser light and therefore unaffected. As the cooling process continues, the distribution of atomic resonance frequencies will shift toward the frequency of the atoms with the central trajectory. To further cool the distribution, the laser frequency needs to be shifted to remain resonant with atoms on the periphery of the velocity distributions. Alternatively, an external electric or magnetic field or both, could be applied to slightly shift the atomic resonance via the Stark or Zeeman effects as the distribution is cooled.

The fact that all real beams have a non-zero spread in atomic velocities slightly complicates the process of spontaneous cooling, because the frequency shift of the atoms depends on their speeds as well as on their trajectories. For example, consider a beam of 250-MeV hydrogen atoms with a Gaussian momentum distribution having an RMS width of $\sigma_p = p \times 10^{-4}$, which is being cooled by means of the Lyman-α transition at 1216 Å. Assume that the angular divergence of the beam is 1 mrad. If the cooling laser is oriented 75° with respect to the atomic beam, the speed variations in the beam result in a variation of 60 GHz in the required resonant laser frequency. The trajectory variations in the beam will require only a 1.6-GHz frequency spread. In short, there is a problem in that the frequency shifts caused by the divergence could be masked by those caused by longitudinal momentum spread.

Fortunately, this problem can be solved by an appropriate orientation of the cooling lasers. If the angle between the beams is chosen to be the so-called "magic angle" θ_m, given by

$$\theta_m = \cos^{-1}(\beta) \quad , \tag{7}$$

the effects of speed variations on the frequency spread in the atoms will be minimized. In the example above, the velocity variations in the beam will then result in a variation of only 8.6 MHz in the laser frequency. The trajectory variations will demand a variation of 2.5 GHz. With a nonrelativistic beam, the magic angle reduces to 90°, as would be expected from Eq. (7).

1.1.1.3. Stimulated Cooling. A disadvantage of the spontaneous cooling mechanism outlined above is that the minimum cooling time is limited to

$$\tau = 2\gamma\ k/v_\perp \quad , \tag{8}$$

where γ is the spontaneous decay lifetime, k is the magnitude of the photon wave vector, and $v_\perp$ is the maximum transverse velocity component of the atomic beam. With an intense laser beam, the stimulated decay rate of the atoms could greatly exceed the spontaneous decay rate. Aspect et al. have demonstrated such a cooling scheme[3] utilizing stimulated emission that reduced the cooling time by an order of magnitude over that achieved by the spontaneous process. Their nonrelativistic approach consisted of passing the atoms through a standing wave that was tuned to the high energy side of an atomic resonance frequency. The standing wave provided a periodic spatial intensity distribution that induced a spatial periodicity in the energies of the atomic states, as illustrated in Figure 4. The admixture of unperturbed atomic states in the dressed |+> and |-> states also shows a position dependence.

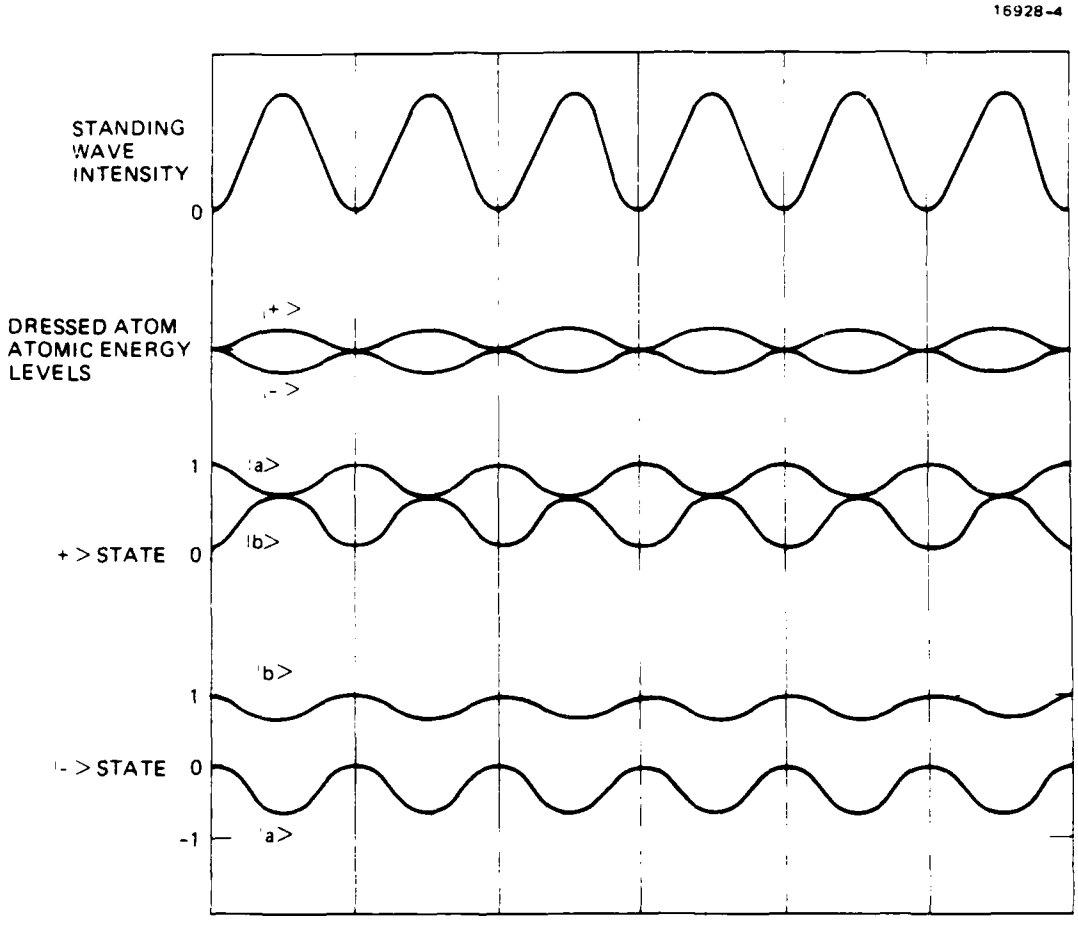

Figure 4. Position-dependence of "dressed" atom energies and states in a standing wave.

Consider an atom with a velocity that has a small transverse component along the periodicity direction of a standing wave. If the atom begins in the $|+,n\rangle$ state at a node of the standing wave, $\cos(\theta)=1$ and the atom is in a pure $|a,n+1\rangle$ state, and at the node of the transverse potential well shown in Figure 4. As the atom adiabatically moves to an anti-node in the distribution, some of the $|b,n\rangle$ state is mixed into the configuration. Spontaneous decay to a $|+,n-1\rangle$ or a $|-,n-1\rangle$ becomes possible. Upon decay to a $|-,n-1\rangle$ state, the atom will again find itself at the bottom of a transverse potential well that it will again climb. The energy required to climb the potential well creates a drag force, which serves to damp out the transverse velocity component of the beam.

This technique shows promise for greatly enhanced cooling rates without saturation. Further research should be pursued on how this method could be applied to cooling a relativistic beam.

1.1.1.4 π-Pulse Cooling. Another way to improve on the cooling rate limit of spontaneous cooling is to stimulate radiative decay rather than wait for the excited state to decay spontaneously.[4] By appropriate selection of the duration and intensity of the cooling pulses, it is possible to obtain a unit probability of a transition from the ground state to the excited state, or vice-versa. Such a pulse is called a π-pulse. Cooling an atomic beam with this technique is illustrated in Figure 5. The atom is originally in the ground state when it is hit with the first π pulse. This pulse gives the atom a unit probability of being in the excited state, and transfers one unit of photon momentum to the atom. A second π-pulse is then applied from the opposite side of the beam to stimulate the atom back down to the ground state. The atomic recoil from the second pulse is in the same direction as the momentum picked up from the first pulse. If the Doppler effect is used to act selectively on only those atoms

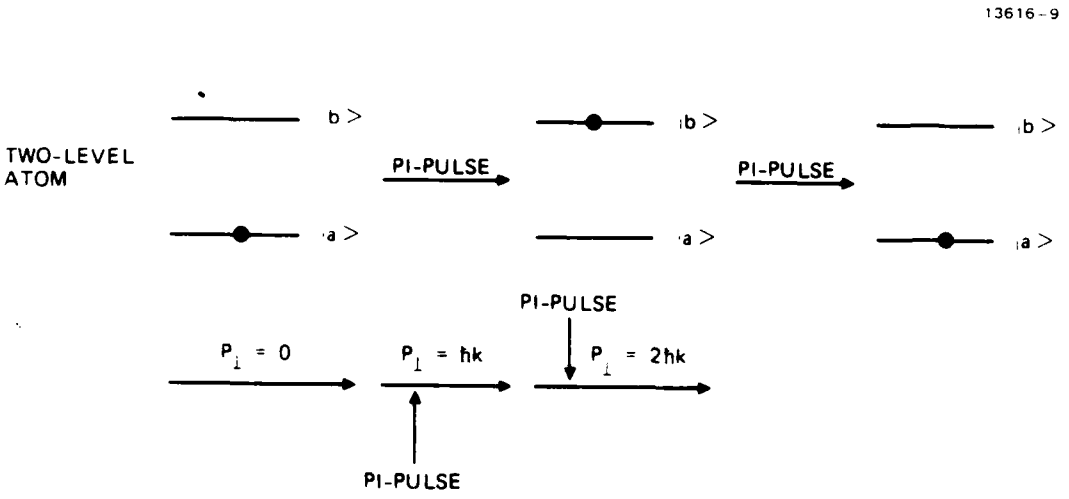

Figure 5. π-pulse cooling scheme. Atoms are hit with a π-pulse while in the ground state, giving them one unit of photon momentum. The atoms are then stimulated back to the ground state from the opposite side, giving them another unit of photon momentum in the same direction.

moving towards the source of the first pulse, this process is very similar to the spontaneous cooling scheme. The π-pulse cooling rate will be given by the stimulated decay rate, which is much faster than the limiting spontaneous decay rate of the spontaneous cooling process.

1.2 APPLICATIONS OF LASER COOLING

There are a number of potential applications of lasers to cooling samples of atomic hydrogen down to milli-Kelvin temperatures. In this subsection we will briefly discuss applications in the areas of neutral particle beam weapons, atomic clocks, and exotic fuels.

1.2.1 Neutral Particle Beam Weapons

Laser cooling of atomic hydrogen is of practical interest in reducing the divergence of the types of relativistic neutral particle beams presently under consideration for weapons applications. As has been outlined in previous publications,[5,6,7] laser cooling can significantly decrease the emittance of relativistic neutral particle beams. This reduction has a large impact on neutral particle beam system design, because a decrease in the divergence angle by a factor F results in an increase in the beam brightness by a factor F^2.

1.2.2 Atomic Clocks

There has been a flurry of recent scientific interest in electromagnetic cooling and trapping of neutral atoms.[3,8,9,10,11] Such trapped atoms open the possibility of developing compact, highly accurate atomic clocks. The ability to cool and trap atomic hydrogen, for instance, would permit incorporation of these capabilities into an extremely stable hydrogen maser.

1.2.3 Exotic Fuels

An Air Force Study conducted by R. L. Forward[12] pointed out the potential benefits of developing propulsion devices that utilize solid antihydrogen as an energy source. The low mass-to-energy ratio of this fuel makes it attractive for propulsion in space environments where the transportation cost per gram of fuel is very high. The proposed techniques for producing solid antihydrogen include laser cooling and trapping of atomic antihydrogen, because the antimatter would react so quickly with the walls of a container made from normal materials. Since the interaction of photons with hydrogen and antihydrogen is expected to be identical, the same technologies for laser cooling and trapping a sample of normal hydrogen can be applied to a sample of antihydrogen.

Another exotic fuel with a high energy-to-mass ratio is a condensed state of hydrogen Rydberg atoms. It has been predicted that a sufficiently dense gas of cold Rydberg atoms will condense to form a collective state that is metastable against decay of the highly excited atoms.[13]

1.3 OTHER VUV SOURCE APPLICATIONS

The development and characterization of our VUV source also has applications in areas other than laser cooling. Two important areas of Air Force interest are H^- production and materials characterization.

1.3.1 H- Production

Theoretical work by Michels and Montgomery[14] has shown that Li^- production in collisions between lithium atoms is greatly enhanced when the lithium atoms are promoted to Rydberg states. The authors suggest that similarly large cross-sections could be

achieved in H^- formation if a high density of Rydberg hydrogen atoms can be formed. We expect our VUV source to easily saturate the n=1 to n=2 transition in atomic hydrogen, making possible the preparation of a dense gas of hydrogen Rydberg atoms. The VUV source will thus enable a dramatic improvement in H^- production in volume ion sources useful for H^- beam sources and fusion plasmas.

1.3.2 Solid State Physics

A number of spectroscopic studies of insulators are needed to further our understanding of the electrical and optical properties of various materials. Optical properties of potential solid state laser hosts, such as our recently developed diamond laser,[15] for instance, would be very interesting. Applicable techniques requiring a laser with the properties of our source include photoemission spectroscopy, photoreflectance spectroscopy, and photoluminescence spectroscopy.

1.4 EXPERIMENTAL RESULTS

The experimental work carried out under this contract consisted of characterizing and optimizing the coherent radiation produced by our VUV system. The VUV output was produced by mixing radiation from two input beams at 3127 and 5454 Å in a mixture of mercury vapor and buffer gas. We studied the effects of varying the input beam intensities and frequencies, the density of the mercury vapor, and the pressure and composition of the buffer gas. These factors affected both the intensity and linewidth of the resulting VUV radiation generated.

In Section 2 of this report, we will describe the experimental techniques used to generate Lyman-α radiation for these studies. We present our experimental results in

characterizing and optimizing our coherent VUV source in Section 3. Section 4 is a list of presentations and publications resulting from work on this contract.

SECTION 2

GENERATION OF LYMAN-α RADIATION

The Lyman-α radiation we studied was produced by the scheme illustrated in Figure 6. The source consisted of two narrowband oscillators amplified in pulsed-dye amplifiers pumped by the outputs of a dual-beam neodymium-doped yttrium-aluminum-garnet (Nd:YAG) laser. The outputs from the amplifiers were combined in a mercury cell to provide the desired Lyman-α pulses.

The narrowband oscillators consisted of two Coherent Model 699-21 ring dye lasers pumped by two Coherent CR-18 argon ion lasers. The first oscillator delivered 500 to 1000 mW of cw light at 5454 Å. The Rhodamine 560 dye was pumped by an argon ion laser operating at 6 W. The second oscillator contained Kiton Red dye and delivered 300 to 500 mW of power at 6254 Å. The Kiton red dye was pumped at 8 to 9 W.

The outputs of the dye lasers passed through optical isolators, each consisting of a pair of polarizing prisms and a Faraday rotator. The beams then entered modified Quanta-Ray PDA-1 pulsed dye amplifiers (PDAs) that were pumped by the doubled (532 nm) outputs of a dual-beam Nd:YAG laser. Required modifications in the PDAs for this application included replacing internal optics, replacing the metal spatial filters with d amond ones, and mechanically improving the pinhole mounts. With these modifications, we were able to get 10 ns TEM_{00} pulses from both PDAs.

We varied the dye concentrations in the various stages of both PDAs to obtain maximum power without undue amplified spontaneous emission. With optimum dye concentrations and input powers, we were able to achieve 30 mJ at 5454 Å and 6.5 mJ at 6254 Å. The radiation at 6254 Å was doubled in a KDP crystal to produce 2.0 mJ of 3127 Å light.

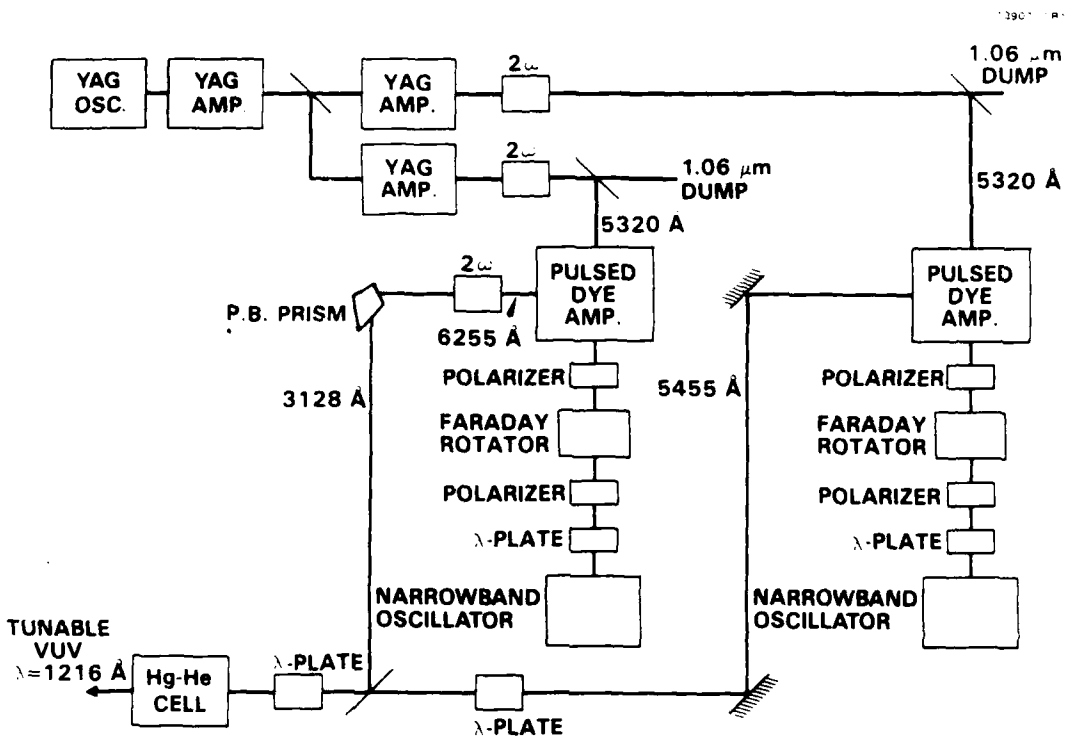

Figure 6. Experimental setup for generation of VUV Lyman-α radiation. The outputs from the dual beam Nd:YAG laser were used as pumps to amplify the outputs of the two narrowband oscillators. The photons at 6255 Å were frequency doubled, yielding photons at 3127 Å. Light at 3127 Å and 5454 Å was combined in a HgHe cell to yield a sum frequency of 1216 Å.

The radiation at 3127 Å was combined with the 5454 Å pulses in the mercury cell, as illustrated in Figure 7. The cell consisted of a center region that was heated to a temperature between 150° and 200°C. During operation, mercury from the wick evaporated and migrated towards the end regions of the cell, which were water cooled. The cooled buffer gas in the end regions condensed the mercury back onto the wicks. The mercury then moved back to the center of the cell where the evaporation/condensation cycle began again. Our interaction region was approximately 5 cm long. As will be explained later, the density of mercury in the cell was monitored by measuring the absorption from a low pressure mercury lamp as a function of cell temperature. After several weeks of operation, we had no accumulation of mercury on the cell windows. However, extended exposure of the LiF exit window to atmosphere resulted in a dramatic decrease in the window transmission at Lyman-α. This has been attributed by other workers to accumulation of water molecules on the LiF surface.

Contamination of the cell by water vapor caused strong absorption of the output beams. We added a cold finger to the buffer gas region of the cell to remove the water but achieved only a limited improvement in the VUV transmission through the cell. Further details of these efforts are given in Section 3.

The mixing process in the mercury cell is illustrated in Figure 8(c). Two photons at 3127 Å were resonant with the mercury transition from the $6s^2\ {}^1S_0$ ground state to the $6s7s\ {}^1S_0$ excited state. The third photon at 5454 Å was nonresonant and could thus be tuned over a broad range. The sum frequency generated by the addition of the three photons was at 1216 Å (Lyman-α).

We observed two competing radiative processes that also occur under these conditions. The first of these was the spontaneous decay at 1.1 μm from the $6s7s\ {}^1S_0$ state to the

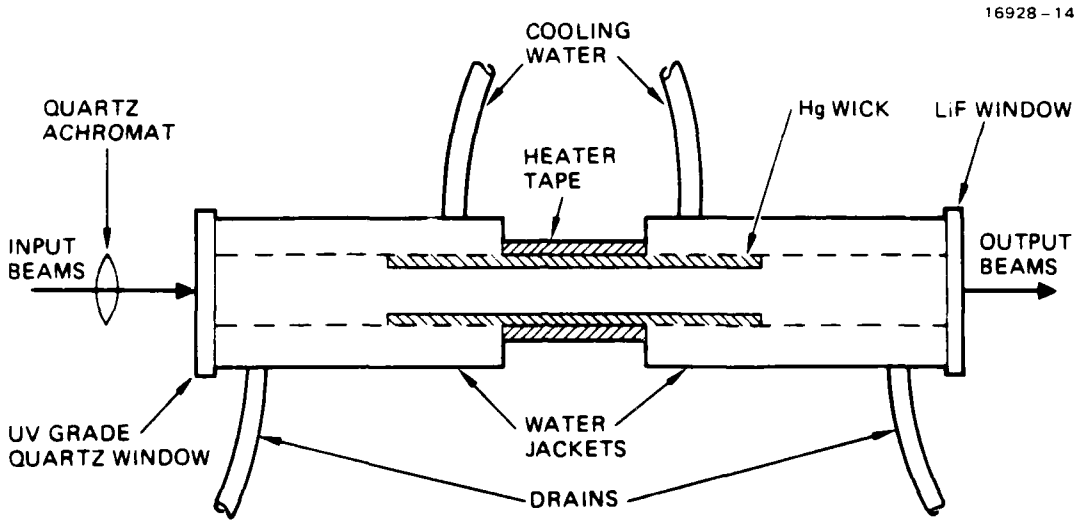

Figure 7. Mercury cell for VUV generation.

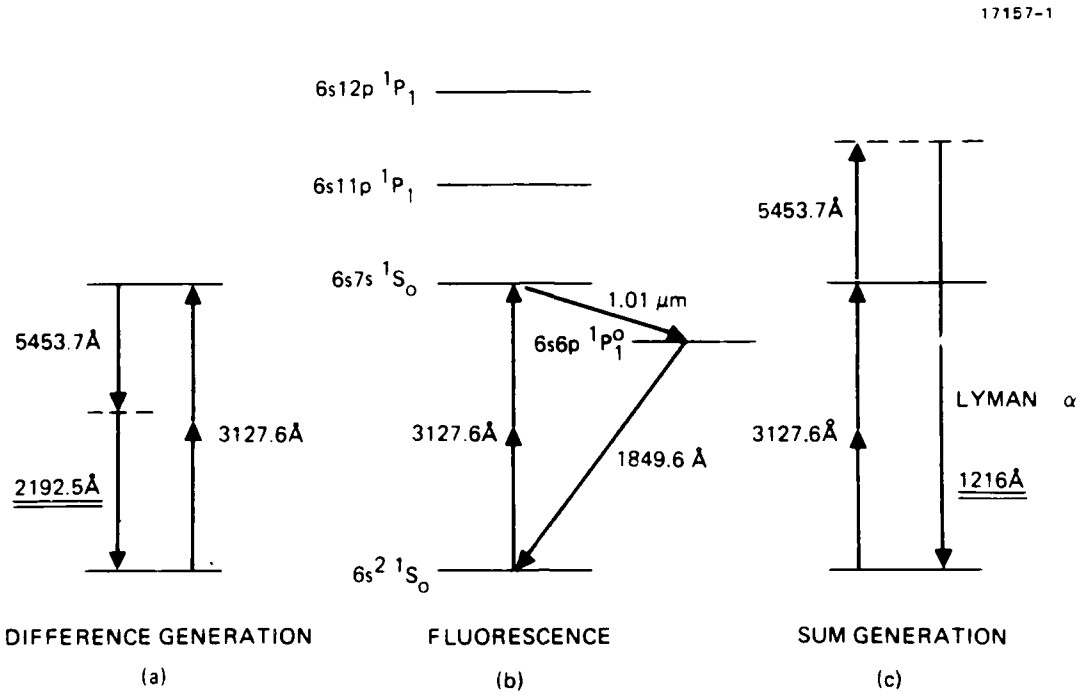

Figure 8. Energy level diagrams in mercury illustrating the three observed frequencies produced under conditions for generating Lyman-α radiation. Figure 8(a) shows the difference frequency generated by combining the energy of two photons at 3127 Å and subtracting the energy of a third photon at 5454 Å. Figure 8(b) shows the fluorescence process where two 3127 Å photons excite the 6s7s ^1S_o state, which spontaneously decays via a two-step process back down to the ground state. Figure 8(c) illustrates the sum frequency generation process which produces Lyman-α radiation by combining the energy of two resonant photons at 3127 Å with a nonresonant photon at 5454 Å.

6s6p $^1P_1$ state, and from there back down to the ground state at 1849 Å, as illustrated in Figure 8(b). Radiation at 1849 Å was strongest when no 5454 Å photons were present. Its intensity was reduced by a factor of 3 to 4 in the presence of the 5454 Å photons needed to permit sum and difference frequency radiation.

The second competing process was the difference frequency generation at 2193 Å, as illustrated in Figure 8(a). The intensity of this radiation can be reduced by a proper choice of phase matching conditions because, as Bjorklund has calculated,[16] it peaks when $b\Delta k=0$.

We have studied the intensities and linewidths of all three of these signals in order to understand the physics of the sum frequency generation process. For instance, the simplicity of the fluorescence process makes it possible to infer information about the population of the 6s7s $^1S_0$ state, which would be difficult to determine from the sum frequency data alone. More details about these measurements are presented in Section 3.

The output of the mercury cell was analyzed using a McPherson Model 225 one meter scanning VUV monochromator. The monochromator was calibrated by using spectral lines from a hydrogen Hinterreger light source at Lyman-α and with a number of mercury lines from a mercury lamp. A portion of the spectrum from the hydrogen discharge source near Lyman-α, is shown in Figure 9.

To prevent stray laser pump light from within the monochromator from reaching the photomultiplier tube, a number of the lines were passed through selective filters at the output of the monochromator. The Lyman-α output from the cell with an Acton Research 122-N-1D notch filter is shown in Figure 10. This filter has a peak transmission at 1200 Å and a bandwidth of 150 Å.

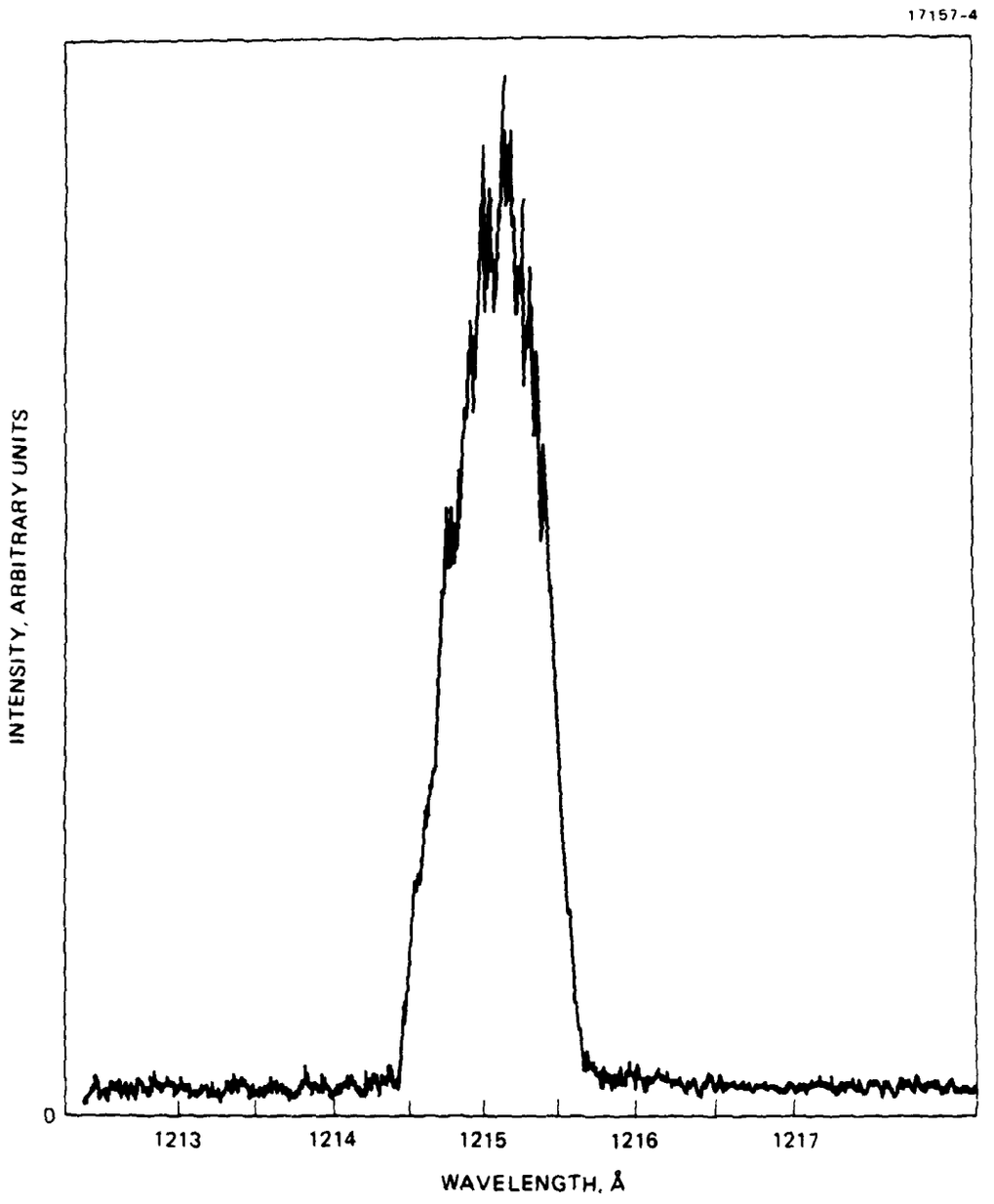

Figure 9. Scan of the Lyman-α line from a Hinterreger hydrogen discharge lamp as measured on the McPherson Model 225 one meter scanning VUV monochromater.

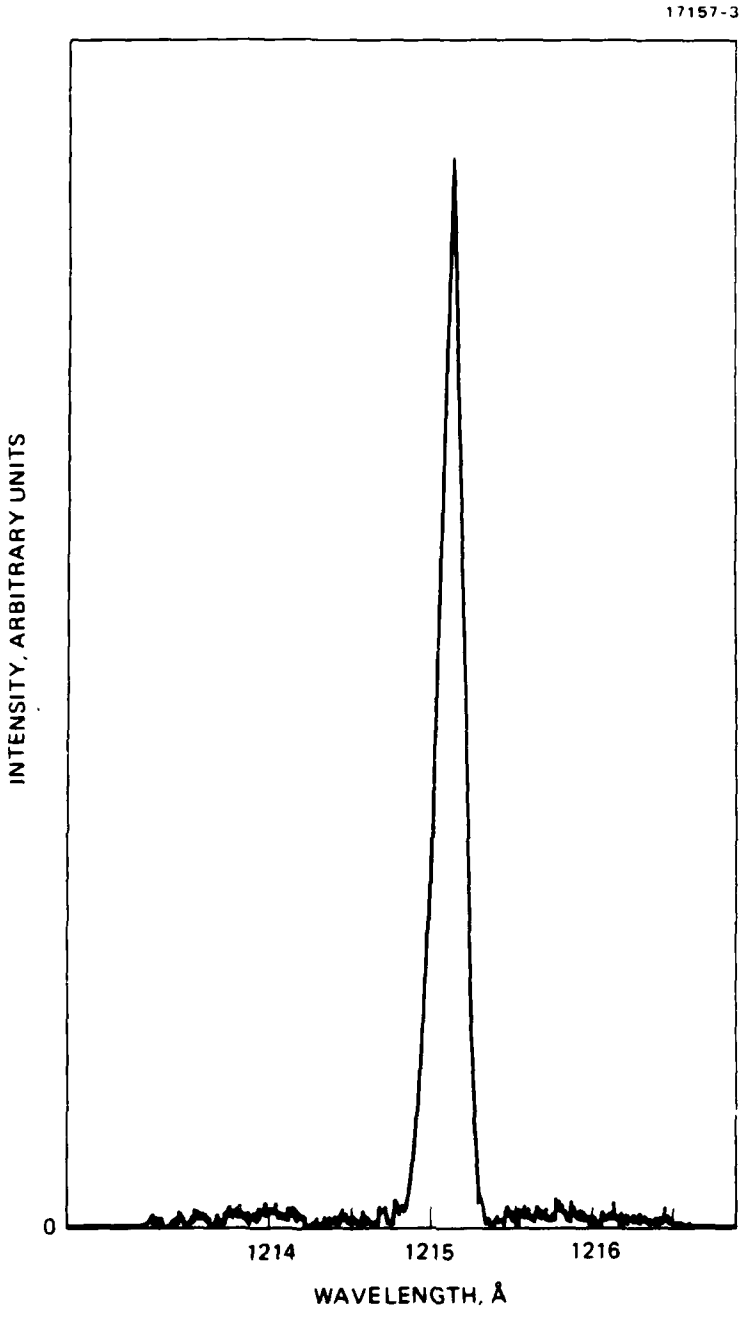

Figure 10. Scan of the mercury cell output at Lyman-α as measured on the McPherson Model 225 one meter scanning monochromator. The width of the line as shown is at the limit of the monochromator resolution. The monochromator output was passed through a Lyman-α notch filter before being detected by the solar blind photomultiplier tube.

In the next section we will discuss the data obtained with this experimental setup. Radiation at 2193, 1849, and 1216 Å were all used to examine the dynamics and limits of the VUV mixing process.

SECTION 3

EXPERIMENTAL RESULTS

Our experimental efforts concentrated on understanding and optimizing the VUV output of our Lyman-α source. To better understand all aspects of the production process we studied the difference frequency radiation at 2193 Å, and the fluorescence signal at 1849 Å, as well as the sum frequency radiation at 1216 Å.

The theoretical output intensity of the sum and difference frequency signals in the absence of saturation effects is given by the expression

$$I_4 \alpha (I_1)^2 I_3 (N\chi^{(3)})^2 F(b\Delta k) \quad , \qquad (9)$$

where I_4 is the intensity of the output beam, I_1 is the intensity of the radiation at 3127 Å, I_3 is the intensity of the radiation at 5454 Å, N is the density of the mercury, $\chi^{(3)}$ is the third order nonlinear susceptibility, and $F'(b\Delta k)$ is a phase matching factor. The parameter b is the confocal beam parameter and Δk is the magnitude of the difference between the vector sums of the wave vectors of the input beams and the wave vector of the output beam. Optimizing the sum frequency output entails maximizing the input intensities, mercury density, and phase matching factors within the limits imposed by saturation, mercury clustering, and ionization. Other radiation processes, such as difference frequency generation and amplified spontaneous emission, need to be minimized so the maximum sum frequency signal is produced.

The form of the phase matching factor depends on the geometry of the system and on the mixing process in question. For difference frequency generation with tightly focused input beams, Bjorklund has calculated[16]

$$F'(b\Delta k) = \pi^2 e^{-b|\Delta k|} \quad . \tag{10}$$

This factor peaks when $\Delta k=0$. The sum frequency phase matching factor is

$$F(b\Delta k) = \begin{cases} 0 & \text{for } \Delta k \geq 0 \\ (\pi b\Delta k)^2 \, e^{b\Delta k} & \text{for } \Delta k < 0 \end{cases} \quad . \tag{11}$$

It is maximum when $b\Delta k=-2$. Thus it is possible to select the phase matching conditions so the sum frequency generation is favored over the difference frequency generation. The phase matching can be changed by slightly detuning the 3127 Å beam from resonance, changing the angles of the input beams with respect to each other, or altering the composition of the buffer gas used in the mercury cell. Krypton, for example, is negatively dispersive in this wavelength region and can be used to make Δk more negative in the cell.

The intensity of the fluorescence signal in the absence of saturation of the population of the 7^1S state is given by

$$I_4 \propto (I_1)^2 N \quad . \tag{12}$$

In fluorescence, the intensity does not depend on the wave vector mismatch between the incident and outgoing waves. As the occupation probability of the 7^1S state approaches 1/2, the fluorescence intensity should be independent of the intensity of the input beam.

3.1 MERCURY DENSITY DETERMINATION

To quantify our measurements, it was necessary to determine the mercury density in the interaction region of the cell. Thus we measured the transmission of a low pressure mercury lamp at 1849 and 2537 Å. We initially expected these measurements to indicate that the mercury pressure in the interaction region was approximately equal to the vapor pressure of mercury at the temperature of the heated region of the cell. In fact, the transmission observed at the highest temperatures was orders of magnitude higher than what one would expect based on our initial vapor pressure assumptions. A representative curve of our transmission measurements is shown in Figure 11.

In order to relate the measured transmission through the mercury cell to the mercury density, we will first present the formulas for the mercury cell transmission, taking into account the non-zero linewidth of the source and the absorber. These formulas involve normalized line shape functions with characteristic widths. The discussion on the line shape functions is followed by the results of fitting the densities to the measured transmission data.

3.1.1 Relationship Between Density and Transmission

The measured transmission through the mercury cell was used to determine the mercury density by means of the equation[17]

$$I = I_0 \int_{-\infty}^{\infty} g_s(\nu) e^{-\alpha(\nu) L} d\nu \ , \qquad (13)$$

where I is the transmitted intensity, I_0 is the intensity in the limit of 0 density, $g_s(\nu)$ is the normalized lineshape function of the source, $\alpha(\nu)$ is the attenuation coefficient, and L is the length of the interaction region (assumed to have uniform density). The attenuation coefficient α is related to the

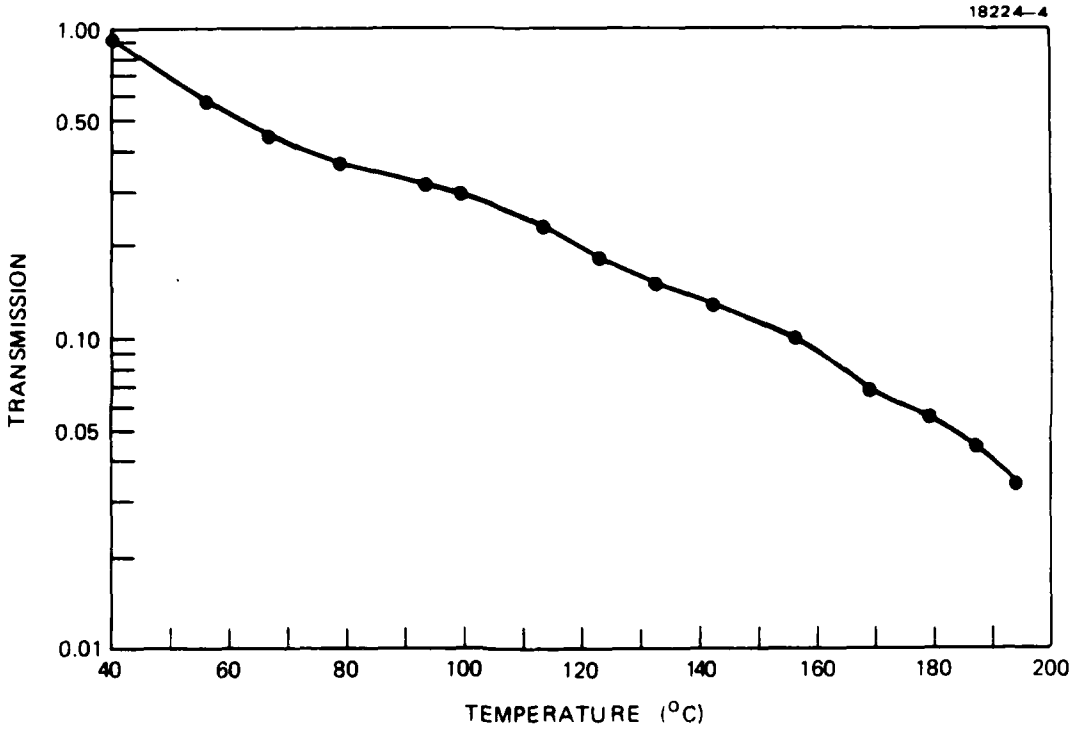

Figure 11. Transmission of light at 2537 Å from a low pressure mercury lamp through the mercury cell as a function of cell temperature.

mercury density N by the formula[17]

$$\alpha(\nu) = \frac{\lambda^2 A_{21} g_2 N}{8\pi\, g_1}\, g_a(\nu) \quad , \tag{14}$$

where λ is the wavelength, A_{21} the Einstein A coefficient, g_1 and g_2 the degeneracies of the respective upper and lower transition levels, and $g_a(\nu)$ the normalized lineshape function of the absorber.

To solve for the density using Eqs. (13) and (14), the interaction length L was taken to be 4.0 cm. The two wavelengths were λ=1849 Å and λ=2537 Å, with respective values of g_2/g_1 being 1 and 3. The values of A_{21} were taken from the literature[18, 19] to be 763 MHz for 1849 Å and 8.69 MHz for 2537 Å.

3.1.2 Normalized Lineshape Functions

The two lineshape functions appearing in Eqs. (13) and (14) were determined by a combination of theory and experiment. The absorption lineshape was assumed to be caused by inhomogenous Doppler broadening with the functional form[17]

$$g_a(\nu) = \frac{2\,(\ln 2)^{1/2}}{\Delta\nu_D\, \pi^{1/2}} \exp\{-[2(\nu-\nu_0)/\Delta\nu_D]^2 \ln 2\} \quad . \tag{15}$$

We used a Voigt profile for the source with a lineshape function of[17]

$$g_s(\nu) = \frac{2}{\Delta\nu_D} \left(\frac{\ln 2}{\pi}\right)^{1/2} \mathrm{Re}[w(z)] \quad , \tag{16}$$

where $z=x+iy$ and $x=(\nu-\nu_0)(\ln 2)^{1/2}/\Delta\nu_D$ and $y=\Delta\nu_N(\ln 2)^{1/2}/\Delta\nu_D$. The linewidths $\Delta\nu_D$ and $\Delta\nu_N$ are the separate contributions of the Doppler broadening and collisional broadening to the total linewidth of the source. The term $w(z)$ appearing in Eq. (15) is $1/i\pi^{1/2}$ times the complex plasma dispersion function.[17]

$$\mathrm{Re}[w(z)] = \frac{y}{\pi} \int_{-\infty}^{\infty} \frac{e^{-t^2}}{y^2 + (x-t)^2}\, dt \quad . \tag{17}$$

3.1.3 Determination Of Source and Absorber Linewidths

We assumed that the total linewidth of the source had homogenous contributions because of collisional broadening and inhomogeneous contributions from the cell's 300°C operating temperature. The linewidth of the absorber was assumed to be dominated by inhomogeneous Doppler broadening.

The Doppler width $\Delta\nu_D$, appearing in Eqs. (15) and (16), is related to the temperature and wavelength of the source or absorber by the expression

$$\Delta\nu_D = 2\nu_0 \left(\frac{2kT}{Mc^2} \ln 2\right)^{1/2} \quad , \tag{18}$$

where c is the speed of light, M is the mass of the mercury atoms, k is Boltzmann's constant, T is the temperature in Kelvin, and $\nu_0=\lambda/c$.

The homogeneous linewidth $\Delta\nu_N$ appearing in Eq. (17) was determined by measuring the total linewidth of the source at 5461 Å with a Fabry-Perot interferometer. Eq. (16) was then solved numerically for $\Delta\nu_N$ using a value for $\Delta\nu_D$ given by Eq. (18). The collisional broadening is determined by the mean time between collisions in the source and is therefore independent of wavelength. The natural linewidth at each line

does depend on wavelength but is much smaller than the collisional linewidth. For this reason, the value of $\Delta\nu_N$ measured at 5461 Å was also used as the homogenous linewidth at 1849 and 2537 Å.

The measured source linewidth at 5461 Å was 3.6 ± 0.1 GHz. The mirror spacing in the Fabry-Perot was varied to give a free spectral range between 7.5 and 30 GHz. The finesse was measured with a laser source to be 30. Figure 12 is a plot of the interferometer output for a 1.0 cm mirror spacing corresponding to a 15 GHz free spectral range.

3.1.4 Fitting the Data

The constants I_0 and N in Eqs. (13) and (14) were adjusted to fit the measured intensity profiles, providing good agreement between the absorption measurements at equal temperatures but different wavelengths. The results of these fits are plotted in Figure 13, which gives the density in our cell as a function of cell temperature.

For most of the measurements reported here, the mercury cell was operated at 180°C. A few of the later measurements were taken at 150°C. Our analysis of the absorption data indicates that these correspond to respective densities of $1.6\text{x}10^{13}$ and $1.0\text{x}10^{13}$ cm^{-3}.

There are orders of magnitude difference between our measured densities and those predicted from assuming the cell pressure is equal to the vapor pressure at a given temperature. We attribute this to the contamination of the mercury by the wick, and the time constant associated with the wicking of the vaporized mercury.

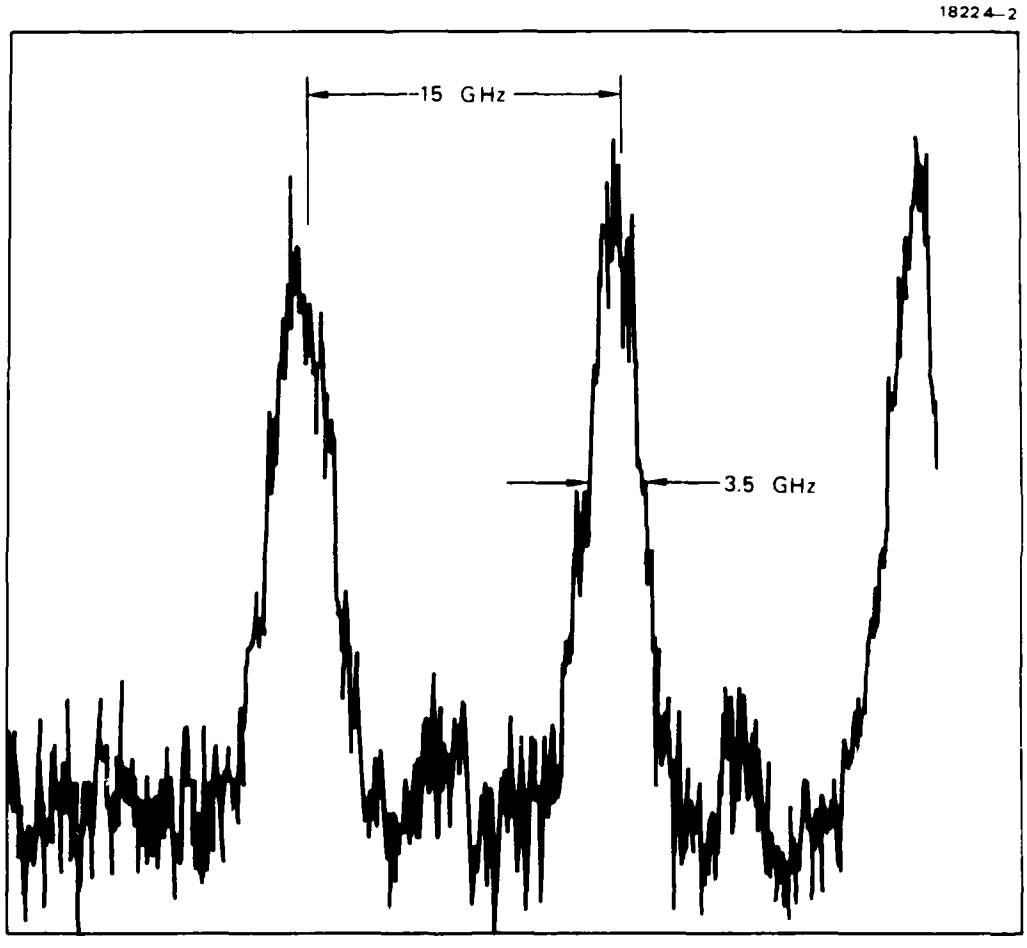

Figure 12. Fabry-Perot interferometer output of the low pressure mercury lamp at 5461 Å. The output was averaged for 20 minutes to improve the signal to noise ratio. The mirror spacing of the interferometer was 1.0 cm corresponding to a free spectral range of 15 GHz. A finesse of 30 was measured with a laser source as input.

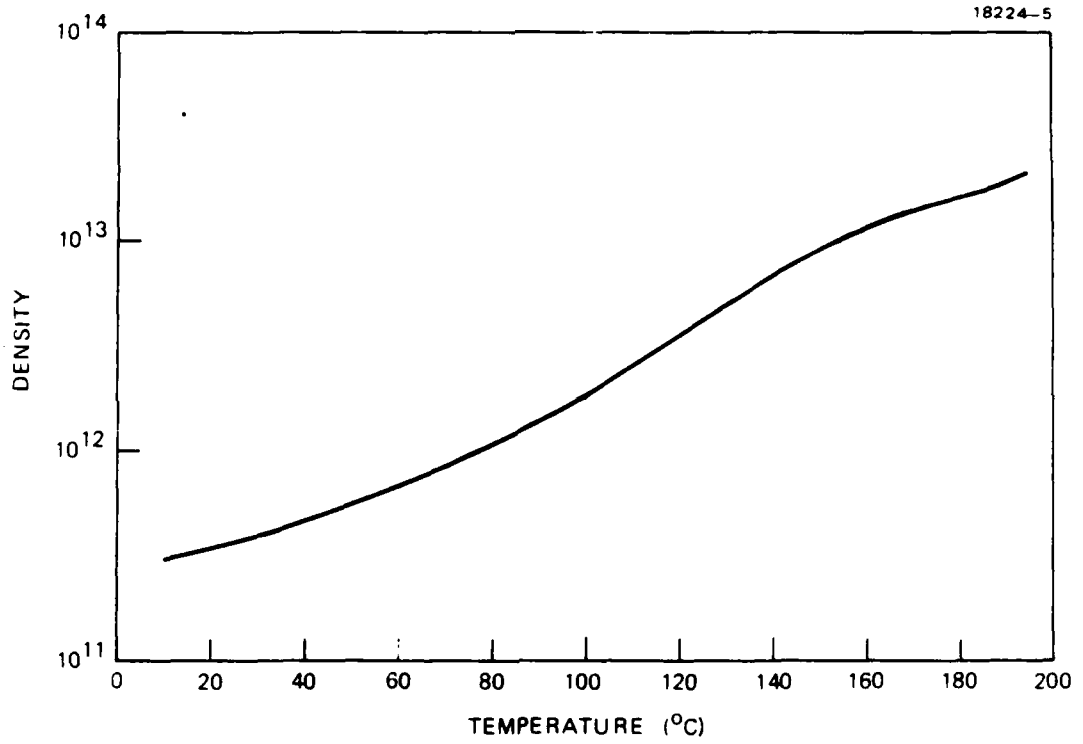

Figure 13. Mercury cell density as a function of cell temperature.

3.2 INTENSITY AND LINEWIDTH OPTIMIZATION OF THE VUV SOURCE

Our measurements showed that the peak Lyman-α intensity occurred when the 3127 Å beam was tuned 0.5 cm^{-1} to the blue of the low intensity resonance wavelength of 31964.1 cm^{-1}. The 1849 and 2193 Å fluorescence signals were maximum when the wavelength of the 3127 Å beam remained fixed at 31964.1 cm^{-1}. The full width at half maximum of the 1849 Å fluorescence signal as a function of the wavelength of the 3127 Å beam was 1.3 cm^{-1}. The fact that this width is much larger than either the Doppler width of 0.03 cm^{-1} or the isotopic shifts of 0.1 cm^{-1} is indicative of power broadening.

Our results can be compared with the measurements of Scheingraber and Vidal[20] for frequency tripling in strontium. They observed that the functional form of the intensity of the tripled output as a function of the frequency of the input beam depended on the intensity of the exciting beam. In their work, the intensity of the input beam was varied between 10^6 and 10^{10} W/cm^2. They also reported a frequency broadening and a blue Stark shift of the resonance frequency similar to what we saw in sum frequency generation. It is not clear why our results do not show a similar resonance shift in difference frequency generation or fluorescence. Mahon and Tomkins[21] also reported an observation of the Stark broadened absorption linewidth in mercury at these intensities, but did not report the blue shift in the resonance frequency that we found.

The blue shift in the pump required to achieve the maximum sum frequency signal can be explained as a saturation of the population of the 7^1S_0 state with increased intensity. $\chi^{(3)}$ for the process of sum frequency generation depends on the difference in population between the 7^1S_0 excited state and the ground state. This difference increases off-resonance under conditions of large input powers. The enhancement is larger to the blue side of the resonance because of phase matching effects.

To further investigate the saturation of the 6^1S to 7^1S transition, we measured the fluorescence signal at 1849 Å as we varied the mercury cell temperature, input beam intensity, and buffer gas pressure and composition. The 1849 Å signal is expected to be proportional to the population of the 7^1S state, because it results from a cascade from the 7^1S state to the 6^1S ground state through the 6^1P state.

The intensity of the 1849 Å fluorescence signal decreased by a factor of 5 when the 5454 Å beam was allowed to pass through the cell in the presence of the 3127 Å beam. This indicates that the population of the 7^1S state is significantly reduced over the population as a result of the 3127 Å beam alone. Similar results were reported by Boyd et al. in sodium.[23] Hence, although Smith et al.[22] observed amplified spontaneous emission at 1.0 μm resulting from 7^1S to 6^1P transitions in a plane wave geometry, we concluded that this will not be a problem for Lyman-α output for the tight focusing geometry used here.

The 1849 Å fluorescence intensity as a function of the frequency of the 3127 Å input beam is shown in Figure 14. As with sum frequency generation, the measured 0.64 cm^{-1} ac Stark broadened linewidth is significantly larger than either the linewidth of the input beam, the Doppler broadening, or the isotopic frequency shifts.

Figure 15 is a plot of the intensity of the 1849 Å fluorescence as a function of mercury density. Increasing the mercury cell temperature beyond 145°C reduces the observed fluorescence output, primarily because of reabsorption of the 1849 Å light by the mercury after the interaction region. Figure 16 is a plot of the data in Figure 15, corrected for the calculated absorption of the 1849 Å light.

We further investigated the saturation of the two-photon absorption by monitoring the 1849 Å fluorescence as a function of input beam intensity. Figure 17 is a representative plot of this

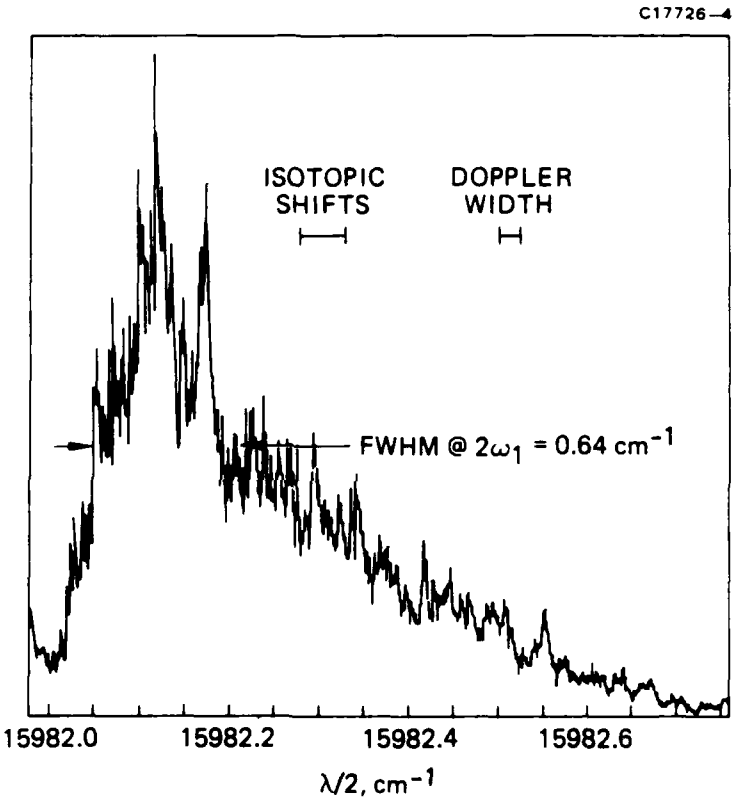

Figure 14. 1849 Å fluorescence as a function of detuning of the 3127 Å beam.

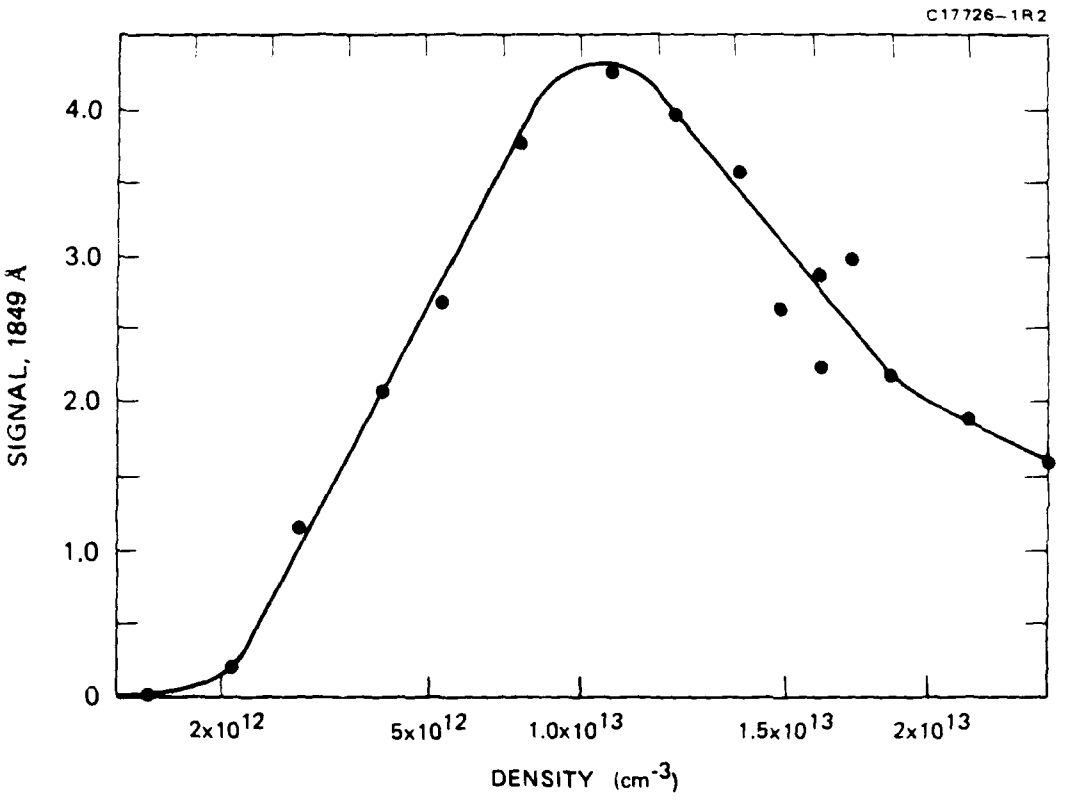

Figure 15. 1849 Å fluorescence as a function of mercury density.

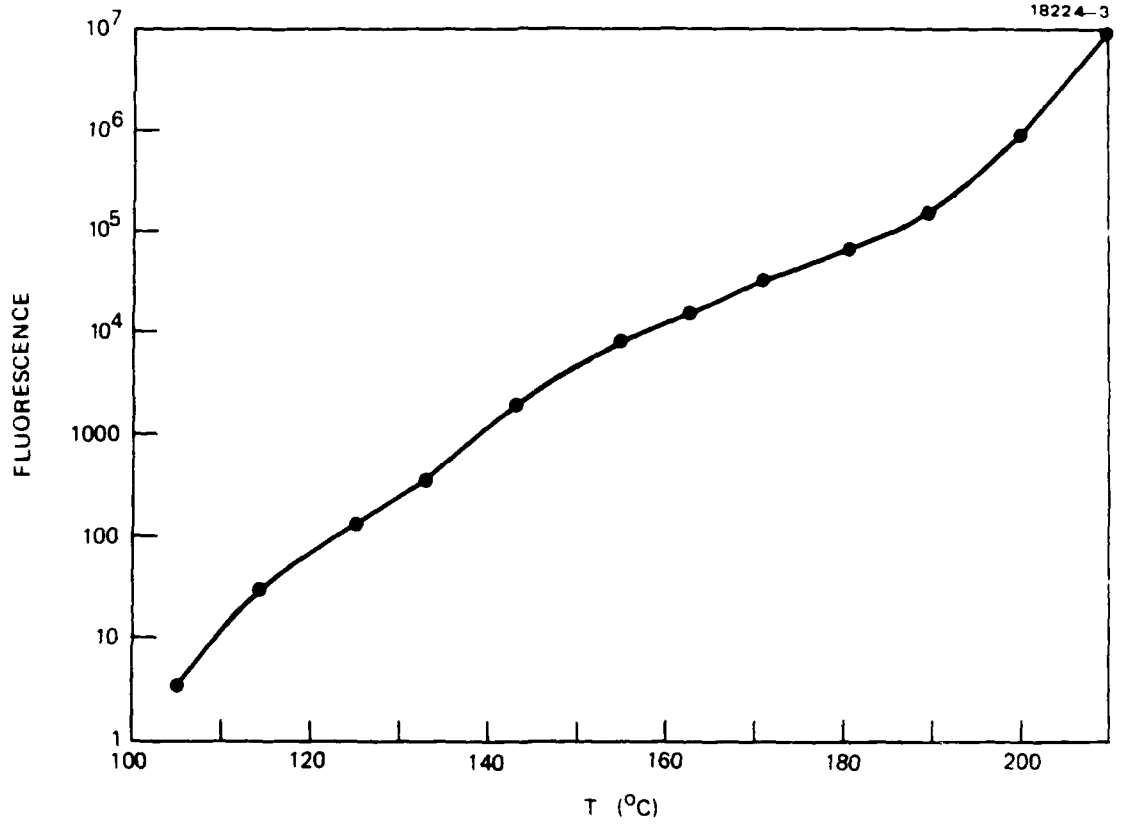

Figure 16. 1849 Å fluorescence as a function of mercury density, corrected for absorption. Except for the absorption correction, these are the same data as presented in Figure 14.

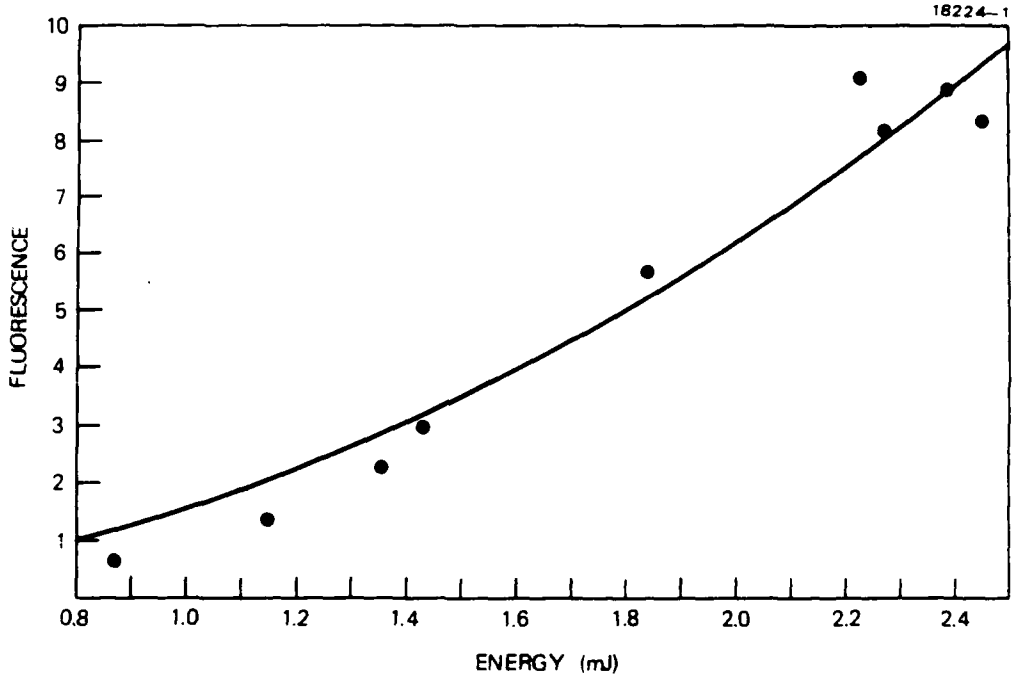

Figure 17. Fluorescence signal at 1849 Å as a function of 3127 Å pulse energy. The solid line is a fit to the data with a function of the form $I=aE^2$, with a=1.55.

signal as a function of the energy of the 3127 Å pulses. The solid curve is a fit to the form $I=aE^2$ with the fitted value of a=1.55. I is the intensity of the fluorescence signal and E the pulse energy. It does not appear to deviate significantly from the low energy quadratic dependence predicted by Eq. (12). If there were a significant occupation of the 7^1S excited state, one would expect the fluorescence intensity to increase less rapidly with energy than quadratically, eventually leveling off to a constant value. The absence of such behavior implies that the cascade from the 7^1S state is sufficiently fast to keep the 7^1S occupation probability close to zero. It is interesting that there is no leveling off of the fluorescence intensity even though the input intensities are large enough to produce significant power broadening and ac Stark shifts.

This observation differs from the behavior observed by Scheingraber and Vidal in strontium,[20] where a dip is seen in third-harmonic generation when the input beams are tuned to the center of the Stark-shifted resonance frequency. Because the third harmonic generation is a function of the population difference between the ground and excited states, Scheingraber and Vidal attribute this dip to significant population in the upper two-photon resonant state.

Figure 18 shows the results of changing the buffer gas from helium to krypton. We observed a slightly less intense 1849 Å signal at a given input power and cell temperature, because of the difference in transmission of the two buffer gases at 1849 Å. The fluorescence had the same functional dependence on the input intensity for both gases. Varying the krypton or helium buffer gas pressure produced no detectable change in the fluorescence. However, we do expect the partial pressure of krypton to have a strong effect on the sum frequency generation. Krypton is negatively dispersive in this wavelength regime and will improve the phase matching conditions of the sum frequency process.

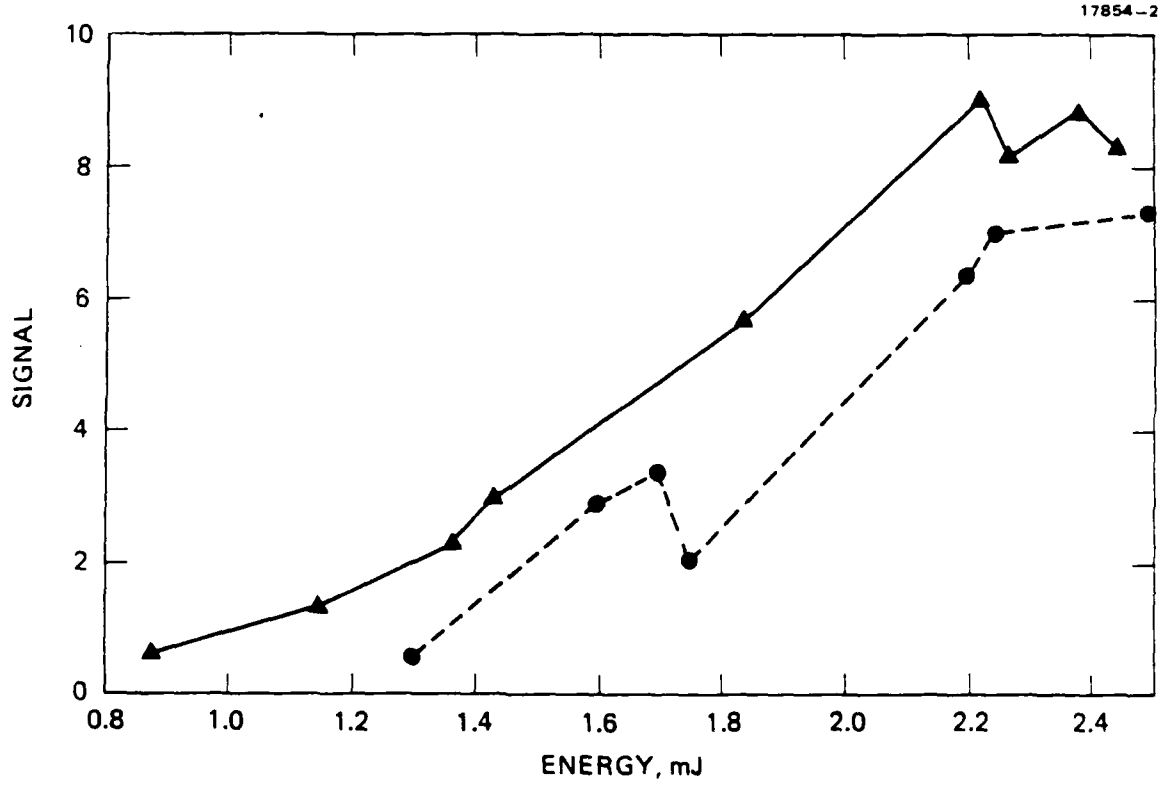

Figure 18. Fluorescence output at 1849 Å as a function of input energy with helium (solid curve) and krypton (dashed curve) buffer gas.

3.3 SUMMARY

In summary, the intensity of our VUV source can be increased substantially without increasing its transform-limited linewidth. We see no evidence of saturation of the output signal when the mercury density is as high as 2×10^{13} cm^{-3}. Input pulses at 3127 Å with energies as high as 2.5 mJ show no onset of saturation for VUV production. This corresponds to a peak intensity of 3×10^{10} W/cm^2 beam intensity. With these high energy pulses, the power broadening of the absorption is sufficiently large to overcome problems that might arise because of Doppler broadening and isotopic shifts in the mercury absorption spectrum. .At the intensity of our 5454 Å beam, very little of the absorbed light at 3127 Å is lost as a result of stimulated or spontaneous decay to the 6^1P_0 state. The difference frequency generation can be minimized by the appropriate selection of buffer gas mixture.

These optimizations have led to the development of a tunable VUV source, which has important characteristics needed in the areas of atomic and molecular spectroscopy, solid state surface studies, neutral particle beam weapons, atomic clocks, exotic fuels, and H^- beam production. The 3 ns transform-limited input beams result in a 2 ns transform-limited output beam with a 250 MHz linewidth. With a 2.5 mJ beam at 3127 Å and a 4 mJ beam at 5454 Å, we estimate an output energy of 2 μJ.

PRESENTATIONS AND PUBLICATIONS

R.S. Turley, R.A. McFarlane, J. Remillard, and D.G. Steel, "Production of intense, coherent, tunable, narrow-band Lyman-alpha radiation," Proc. SPIE, OE/Lase, Los Angeles, Calif., 1988.

R.S. Turley, R.A. McFarlane, and D.G. Steel, J. Remillard, "Production of intense, coherent, tunable, narrow-band Lyman-alpha radiation," AIP Conference Proceedings, Advances in Laser Science-III, Atlantic City, N.J., August, 1987.

REFERENCES

1. J. Dalibard and C. Cohen-Tannoudji, "Dressed-atom approach to atomic motion in laser light: the dipole force revisited," JOSA **B2**, 1707 (1985).

2. J.V. Prodan, A. Migdall, W.D. Phillips, I. So, H. Metcalf, and J. Dalibard, "Stopping atoms with laser light," Phys. Rev. Lett. **4**, 992 (1985).

3. A. Aspect, J. Dalibard, A. Heidmann, C. Salamon, and C. Cohen-Tannoudji, "Cooling atoms with stimulated emission," Phys. Rev. Lett. **57**, 1688 (1986).

4. A.J. Palmer and J.F. Lam, "Radiation cooling using π pulses," JOSA **B3**, 719 (1986).

5. "Experimental and theoretical studies and laser cooling and emittance control of neutral beams," Hughes Proposal Number 81M-0422/E9915, submitted to Air Force Office of Scientific Research, March, 1981.

6. "Experimental and theoretical studies and laser cooling and emittance control of neutral beams," Hughes Proposal Number 82M-4331/EW9915-1, submitted to Air Force Office of Scientific Research, December, 1982.

7. "Experimental and theoretical studies and laser cooling and emittance control of neutral beams," Final Report on Air Force Contract F49620-82-C-0004, 27 January 1987.

8. J. Prodan, A. Migdall, W.D. Phillips, I. So, H. Metcalf, and J. Dalibard, Phys. Rev. Lett. **54**, 992 (1985).

9. W. Ertmer, R. Blatt, J.L. Hall, and M. Zhu, Phys. Rev. Lett. **54**, 996 (1985).

10. R. Blatt, W. Ertmer, P. Zoller, and J.L. Hall, Phys. Rev. **A34**, 3022 (1986).

11. S. Chu, J.E. Bjorkholm, A. Ashkin, and A. Cable, Phys. Rev. Lett. **57**, 314 (1986).

12. R.L. Forward, "Prospects for antiproton production and propulsion," Proc. Cooling, Condensation, and Storage of Hydrogen Cluster Ions Workshop, Menlo Park, Calif., 1987.

13. G. Vitrant, J.M. Raimond, M. Gross, and S. Haroche, J. Phys. **VBV15**, L49 (1982)][REF=E.A. Manykin, M.I. Ozhovan, and P. P. Poluetkov, Sov. Phys. JETP **57**, 256 (1983).

14. H.H. Michels and J.A. Montgomery, Jr., "Negative ion formation in lithium atom collisions," Proc. 4th International Symposium, Brookhaven (1986).

15. S.C. Rand and L.G. DeShazer, Opt. Lett. **10**, 481 (1985).

16. G.C. Bjorklund, "Effects of focusing on third-order nonlinear processes in isotropic media," IEEE J. Quantum Electron. **QE-11**, 287 (1975).

17. C.C. Davis and R.A. McFarlane, "Lineshape effects in atomic absorption spectroscopy," J. Quant. Spectrosc. Radiat. Transfer **18**, 151 (1977).

18. A.L. Osherovich, E.N. Borisov, M.L. Burshtein, and Ya.F. Verolainde, "Radiative lifetimes of levels of the mercury atom," Opt. Spectrosc. **39**, 465 (1975).

19. A. Lurio, "Lifetime of the $6s6p\,^1P_1$ state of mercury," Phys. Rev. **140**, A1505 (1965).

20. H. Scheingraber and C. R. Vidal, Opt. Commun. **38**, 75 (1981).

21. R. Mahon and F. Tomkins, IEEE J. Quantum Electron. **QE-18**, 5 (1982).

22. A.V. Smith, G.R. Hadley, P. Esherick, and W.J. Alford, Opt. Lett. **12**, 708 (1987).

23. R.W. Boyd, M.S. Malcuit, D.J. Gauthier, and K. Rzazewski, "Competition between amplified spontaneous emission and the four-wave-mixing process," Phys. Rev. **A35**, 1648 (1987).


DAT
ILM